Experimental study of self-sustained oscillations in a confined jet

A. Maurel,[1,2] P. Ern,[1,2] B. J. A. Zielinska,[1,2] and J. E. Wesfreid[1]
[1]*Laboratoire de Physique et Mécanique des Milieux Hétérogènes URA CNRS 857, Ecole de Physique et Chimie Industrielles de Paris (ESPCI), 10 rue Vauquelin, 75231 Paris Cedex 05, France*
[2]*Schlumberger Industries/Gas Engineering Montrouge, Boite Postale 620 05-92 542 Montrouge, Cedex, France*
(Received 3 January 1995; revised manuscript received 9 May 1996)

We present an experimental study of a planar jet confined in a rectangular cavity. In certain geometrical configurations and for sufficiently large Reynolds numbers, this system exhibits self-sustained oscillations characterized by a well-defined wavelength and frequency of the jet. We describe flow regimes observed by varying the Reynolds number and the cavity length. The self-sustained oscillation regime is studied in detail: we extract the fundamental frequency and determine the selection criterion for the wavelength using a method of visualization, which has the advantage of being non intrusive. We show the existence of a band of allowed wavelengths and establish the upper and lower limits for the wavelength selection criterion. We discuss the validity of the visualization method for the measurement of the wavelength and frequency using a simple analytical model of the streaklines. [S1063-651X(96)02309-4]

PACS number(s): 47.60.+i

I. INTRODUCTION

Flows in a cavity type geometry belong to a class of flows susceptible to generating self-sustained oscillations. These configurations are usually called impingement geometries because they contain an obstructed shear layer. Since the first observations of the jet-edge oscillations by Sondhauss in 1854 [Fig. 1(a)] [1], many theoretical and experimental studies have been carried out on impinging jet systems. Reviews of principal results for various geometrical configurations have been given by Rockwell and Naudasher [2] and by Blake and Powell [3].

The whistling teapot and the whistle [examples of the hole-tone configuration on Fig. 1(b)] are among the most ordinary examples of such configurations, and common experience suggests a production of discrete tones by these systems. This kind of flow is also present in various wind instruments [Fig. 1(c)] [4] and in many engineering devices; for example, they have been studied as the source of noise in wind tunnels [5,6] and in interaction with combustion in propellers [7]. More recently, flow meters using confined jet oscillations, also called fluidic oscillators, have been developed [see Fig. 1(d) and [8,9]]. These oscillators exhibit robust self-sustained oscillations, with frequency proportional to the flow velocity in a wide range of flow rates [9].

Contrary to the convective instability of a free jet [10], confined jets exhibit well-organized oscillation patterns. It is widely accepted in the literature that the appearance of this globally organized phenomenon observed in confined geometries is due to a feedback effect. Initial flow disturbances grow while being convected by the flow, and interact with the impingement point. This interaction affects the flow by producing a feedback that results in a periodic cycle. In some problems, the feedback is hydrodynamic through the back flow and can be modeled with a Landau model as in the nonlinear delay saturation model proposed by Villermaux and Hopfinger [11] in the configuration of the sudden expansion [Fig. 1(b)]. Other models include acoustic feedback, where the impingement acts as an acoustical dipole source [12]. In many impingement phenomena, the relative strength of the two feedback mechanisms is not yet clearly understood. Chanaud and Powell [13] suggest that both paths, hydrodynamic or acoustic, are possible and that any one can dominate the system. However, the structures observed in all cases are clearly due to a mechanism connected to confinement. Indeed, while the wavelength of the so-called free jet preferred mode is related only to the nozzle width, the wavelength corresponding to self-sustained oscillations is always connected to the impingement length [14].

A relation between the wavelength of the oscillations λ

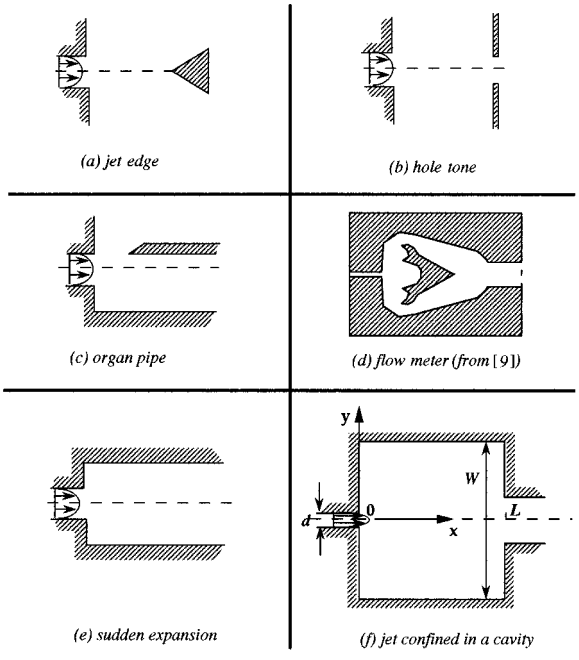

FIG. 1. Configurations susceptible to develop self-sustained oscillations: (a) jet-edge configuration, (b) hole-tone configuration, (c) wind instrument: organ pipe, (d) flow meter configuration (from [9]), (e) sudden expansion, (f) configuration of the present study: jet confined in a rectangular cavity.

and the impingement length L, typically obtained in self-oscillating systems, is of the form $L=(N+\epsilon)\lambda$, where N is an integer and $\epsilon<1$ is often called the end correction. Many interpretations of the coefficient ϵ have been proposed ([15–18]). This relation is discussed in Sec. V, where we obtain $\epsilon=1/4$ for our configuration using a visualization method. In addition, we establish the wavelength selection criterion.

In all the impingement systems, different oscillation modes have been observed, but the transition from one mode to another is not fully understood. A hysteresis phenomenon has been suggested in the case of the jet edge [19], but none has been observed in the case of the half cavity [20] and the wedge [21]. This problem is of great importance for the wind instruments where the so-called ''attack transients'' are known to present a complex behavior [4]. Some studies based on the spectral frequency analysis in these systems show a coexistence of various dominant frequencies [22], as was also observed in impinging jets by Ho and Nosseir [23].

In the present work we consider a two-dimensional jet issuing from a nozzle into a rectangular cavity [24,25]. This geometry (Figure 1f) combines features of the sudden expansion and of the hole-tone. In Sec. II, we present the experimental set-up and the visualization methods used to analyze the oscillations. In Sec. III, we describe the different regimes observed when the two parameters, the Reynolds number Re (Re$=U_{\max}d/\nu$, where $U_{\max}$ is the maximum velocity at the jet entrance, d, the nozzle width and ν the kinematic viscosity) and the ratio L/d where L is the distance between the jet nozzle and the cavity exit (the impingement length) are varied. In Secs. IV and V, the spatial wavelength and temporal frequency of the periodic flow are studied in detail. We establish the domain of existence of cavity oscillations as a function of two control parameters: the impingement length L scaled with the nozzle width d and the Reynolds number Re. We show that the nozzle width d selects only a band of wavelengths within all the values allowed by the boundary conditions. In Sec. VI, the phase velocity measurements obtained from streak-line wavelengths are presented and compared with the configurations of the free jet and the mixing layer. The validity of the method based on visualization is discussed in Sec. VII. It is well known that in unsteady flow the streak lines observed by visualization do not coincide with the stream lines. Using a simple analytical model of the streak lines we show that their phase velocity (wavelength) is approximately 7% smaller (higher) than the phase velocity (wavelength) of the true streamlines.

II. EXPERIMENTAL SETUP AND INSTRUMENTATION

The experiments were performed in a gravity driven low velocity water flow loop, which includes the test cavity and a 30-l constant level container. This setup, preferred to the use of a pump, limits parasite frequencies that might perturb the flow. A metallic sponge was placed at the entrance of the 300-mm-long straight PVC duct upstream of the nozzle to break the secondary Dean flows created in the upstream pipe bends. The flow rate was regulated with needle valves and measured with two rotameters placed after the jet chamber to avoid perturbations due to the rotation of the floats. These flow meters have an accuracy of 1% full scale and cover a range of flow rates from 10^{-4} to 3.10^{-2} 1/sec, corresponding to Reynolds numbers of 5 to 1110. The flow rate measurement is obtained with a total accuracy of around 1.5%.

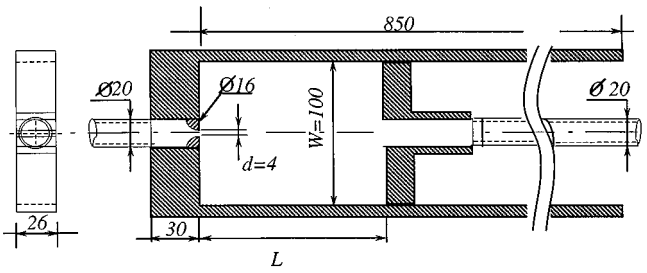

FIG. 2. Geometry of the variable length cavity (dimensions in mm).

The variable length cavity is presented in Fig. 2. It is a rectangular box 100 mm wide and 26 mm high whose length can be regulated with a piston to a maximum length of 850 mm. The jet enters the cavity through a convergent nozzle consisting of two quarter-circles of diameter 16 mm, and exits by a rectangular channel 20 mm wide and 40 mm long. The streamwise velocity profile at the nozzle was measured using laser Doppler velocimetry. We obtained the quasiflat nondeveloped profile shown in Fig. 3. The mean velocity at the entrance, defined as $U_{\text{mean}}=Q/S$, where Q is the flow rate and S is the cross section at the entrance, corresponds to $0.9U_{\max}$ in the range of the explored flow rates.

Visualization experiments were performed using laser induced fluorescence (LIF). The use of this technique is very classic for the study of the dynamical behavior of such a system. For example, Dahm and Dimotakis [27,28] use LIF for the characterization of large-scale turbulent jet. The tracer agent is fluorescein taken at a concentration smaller than 0.1 g/l, so that the mixture density does not present significant stratification. After the test chamber is filled with the dye solution, the oscillations are visualized by a jet of pure water entering the chamber at a desired Reynolds number. This procedure is advantageous because it does not introduce perturbations due to the injection of fluorescein during the observation. Moreover, we observed that the experimental procedure of a fresh water jet in the cavity filled with fluorescein gives a higher contrast for a longer time compared with the alternative procedure of a fluorescein jet in a cavity filled with water. This could possibly be explained by the increase of the effective mass dispersion with the jet velocity in the last case. The plane of observation is obtained with a laser sheet of about 0.5 mm thickness. The

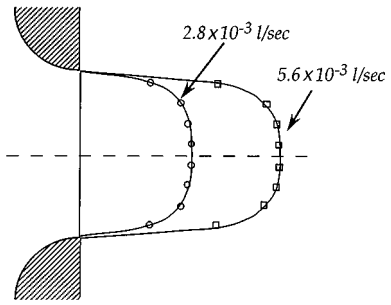

FIG. 3. Velocity profiles at the jet nozzle for flow rates of 2.8×10^{-3} 1/sec and 5.6×10^{-3} 1/sec.

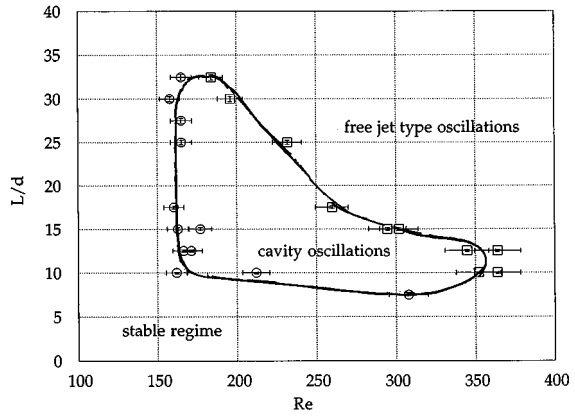

FIG. 4. Flow patterns observed varying L/d and the Reynolds number Re.

sheet is created with a 480-nm argon laser and a vertical cylindrical glass bar. The laser sheet illuminates the test section (x-y) plane in Fig. 1(f) at constant height, generally at half height of the cavity.

The flow patterns were recorded using a charge-coupled device video camera and a digital imaging process. The oscillations were characterized using a spatiotemporal representation. In this representation the image intensity along a chosen line is recorded at successive times, so that the horizontal axis corresponds to the stored line and the vertical axis to the time. For the frequency extraction, a line perpendicular to the jet axis is chosen: the oscillatory motion of the jet center line (in black in the picture on Fig. 9) is stored as a function of time, which allows one to measure the period of oscillation. A similar procedure, with the chosen line being the axis of the jet, has been used to extract the wavelength (see Sec. IV).

III. OBSERVED FLOW PATTERNS

Figure 4 shows a flow pattern diagram as a function of the control parameters: the ratio L/d and the Reynolds number Re. At small values of Re and L/d, we observe a stable regime with two recirculation regions [Fig. 5(a)]. Increase of Re or L/d induces a transition to an oscillatory state [Fig. 5(b)]. At still higher Reynolds numbers or L/d, we observe an evolution to the turbulent behavior of free jets [Fig. 5(c)].

In principle, the flow in the cavity may be three dimensional because of its finite height. We have checked that, in the self-sustained oscillation regime, the flow is mainly two dimensional. Visualizations performed by varying the laser sheet position across the height of the cavity result in similar patterns.

For a fixed geometry, the onset of oscillations in a sinuous form with well-defined wavelength and frequency takes place at the critical Reynolds number [Fig. 5(b)]. The amplitude of the oscillations grows in the downstream direction, similarly to instabilities in open flows with spatial growth of perturbations. However, the corresponding wavelengths are very different from the free jet situation. Unstable structures in the free jet are of the order of the nozzle width, while we will see that, in our case, the wavelength scales with the cavity length. With further increase in the Reynolds number or in L/d value, patterns of free jet type appear in the flow. In Fig. 5(c), an oscillation in varicose mode can be seen with a wavelength of the order of the nozzle width. If the Reynolds number is increased further, a transition to turbulence occurs. At this stage the cavity oscillations have disappeared altogether and we observe free jet type behavior, where varicose structures occur near the jet nozzle and spatially evolve to a turbulent flow further downstream. It can be therefore concluded that, with increasing Reynolds number or L/d value, the influence of the confining cavity becomes weaker until there is nearly no influence for the turbulent jet.

IV. SELF-SUSTAINED OSCILLATIONS: STUDY OF THE WAVELENGTH

Self-sustained oscillations are characterized by a global organization. In this case, the jet oscillates with a well-defined oscillation period and presents a regular pattern. Due to the boundary conditions of the cavity, a wavelength selection occurs.

A. Extraction of the wavelength

We have measured the wavelength using a wavelength extraction procedure from Sec. II. Figure 6(a) shows an instantaneous image of the oscillating jet, for $L/d=25$ and Re $=250$. Here, the x axis is the line of image acquisition. Figure 6(b) shows the corresponding spatiotemporal representation. In this way the structures traveling along the center line were stored as a function of time. In the downstream half of the cavity, the structures corresponding to the interception of the oscillating jet with the center line move with a constant propagation velocity forming a straight line in the spatiotemporal representation. This procedure is inaccurate in the first half of the cavity, where the oscillation amplitude is small. In this part of the cavity, the line chosen for the acquisition lies within the jet thickness and we observe a dark trail on the spatiotemporal diagram. The line obtained in the second half of the cavity is extrapolated towards the entrance of the jet as shown on Fig. 6(b). In this representation, half a wavelength corresponds to the horizontal distance between two straight lines since the jet intercepts the center line each half wavelength. From Fig. 6(b), it appears that the wavelength λ is a fraction of the cavity length: in this case the cavity contains four integer wavelengths plus an end correction of around a quarter of wavelength ($\lambda \sim 23$ mm).

The above procedure uses the streak lines and it is well known that, for unsteady flow, streak lines and stream lines do not coincide [26]. We show in Sec. VII that the wavelength measured from the streak lines wavelength is around 7% higher than the true wavelength of the stream lines.

B. Wavelength selection

Wavelength measurements have been performed by varying the impingement length L and the Reynolds number. In all cases the cavity contains an integer number N of wavelength plus an end correction of around a quarter of a wavelength. We conclude that the mode N corresponds to a wavelength characterized by N in the relation $L=(N+\epsilon)\lambda$, with $\epsilon=1/4$. This law remains valid for all cavity lengths L and

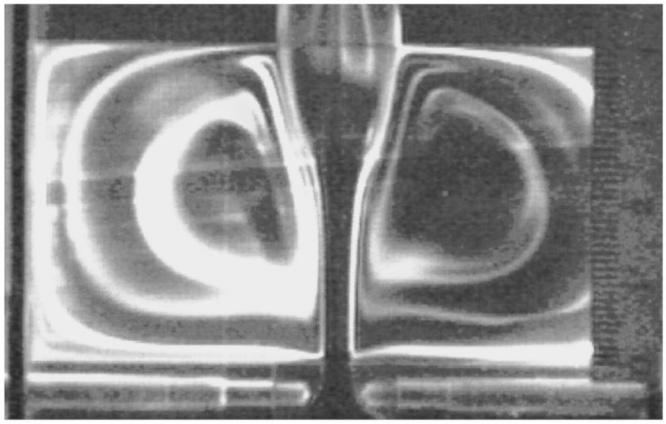

(a)

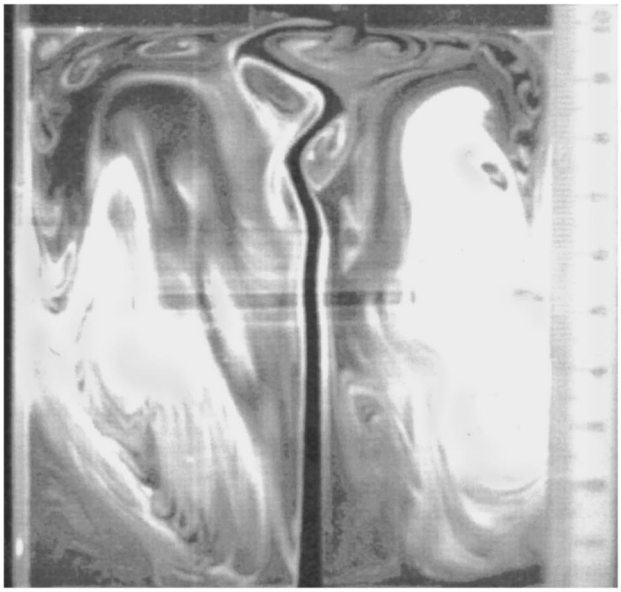

(b)

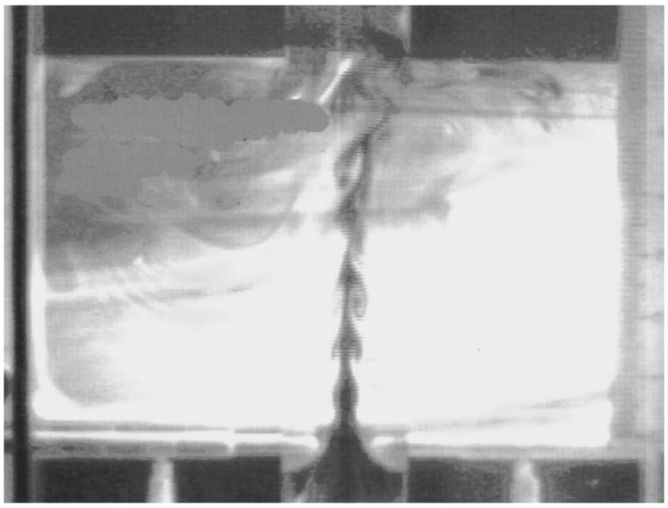

(c)

FIG. 5. Flow visualizations corresponding to (a) stable regime, (b) cavity oscillations, (c) free jet type oscillations.

we note that N increases as L increases. On the other hand, in a given geometry, an increase of the Reynolds number can induce a jump to a higher mode. A longer cavity contains more wavelengths, and higher jet velocity corresponds to smaller structures. The measurements performed for L/d varying between 10 and 30 and Reynolds numbers from 160 to 360 give values of N between 1 and 5. λ is estimated with an experimental accuracy of $\pm 5\%$, the error being mainly

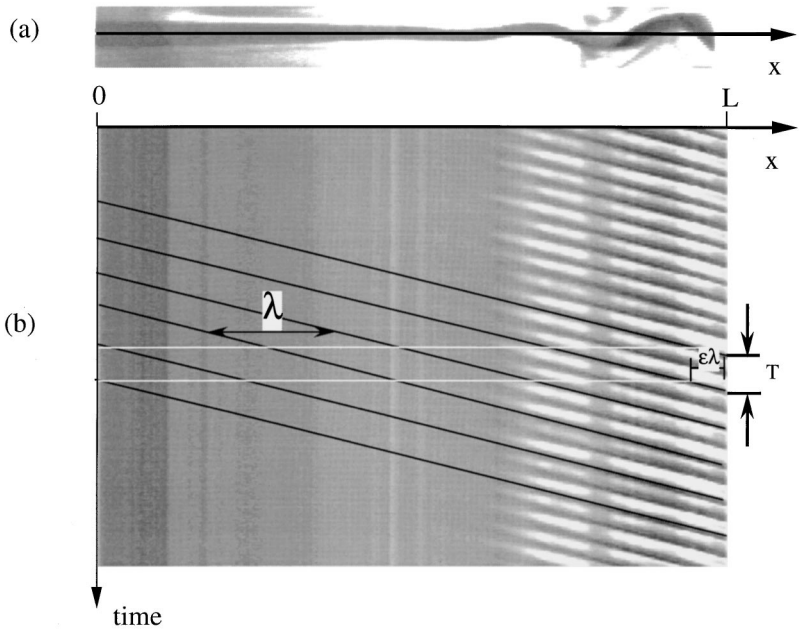

FIG. 6. For Re=250 and $L/d=25$, (a) instantaneous image of the oscillating jet on center line; the x axis corresponds to the line chosen for the spatiotemporal acquisition, (b) spatiotemporal acquisition.

due to the determination of the line slope from the spatiotemporal representation. The experimental error in the determination of the wavelength does not influence the identification of the mode N.

The values found for ϵ were obtained with the same accuracy as λ, varying L and the Reynolds number, with no significant variation. Figure 7 presents the domain of existence of each mode as a function of the Reynolds number and of the ratio L/d. The solid line represents the domain of existence of the cavity oscillation from Fig. 4. This global domain is divided into subdomains of existence of each mode (dashed lines).

C. Wavelength band value

For a given geometry, the system does not select all the N values allowed by the boundary conditions. For example, for $L/d=25$, only modes III and IV are observed (see Fig. 7). To determine the pertinent parameters for this selection, we have changed the cavity width W and the nozzle width d.

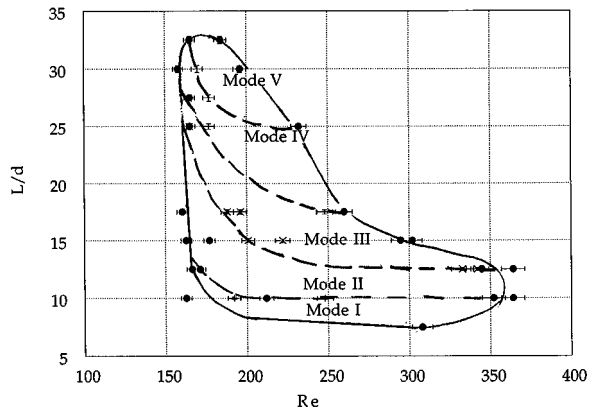

FIG. 7. Stability domains for each mode in the (L/d, Re) plane.

For $L=100$ mm ($L/d=25$), W was changed from 100 to 80 mm by placing thick plates of Plexiglas against the lateral walls. Results show that this parameter has no significant influence on the wavelength selection. The first unstable mode is always the mode II. However, we observed a change of the critical Reynolds number (for $W=100$ mm, $\mathrm{Re}_c=160$, for $W=90$ mm, $\mathrm{Re}_c=182$ and for $W=80$ mm, $\mathrm{Re}_c=186$), suggesting that the lateral confinement stabilizes the flow.

The nozzle width d was changed from 4 to 7 mm for $L=100$ mm by adapting the radius of the quarter circles forming the jet entrance (see Fig. 2). The change observed when d increases are shown in Table I. For a higher value of d, the first unstable mode appears with lower N (corresponding to larger wavelength). We observe, depending on the Reynolds number, the modes III or IV when the jet width at the entrance is smaller than 6 mm and the modes II and III as soon as this width is larger than 6 mm. This means that a thinner jet oscillates with a smaller wavelength. On the other hand, we did not observe any influence of the parameter d on the critical Reynolds number.

The results on the wavelength selection are summarized in Fig. 8. We have represented the nondimensional wavelength λ/d as a function of L/d. All selected wavelength

TABLE I. Modes selected for various d ($L=100$ mm).

d (mm)	First unstable mode	Second mode observed increasing Re
4	III	IV
5	III	IV
6	II	III
7	II	III

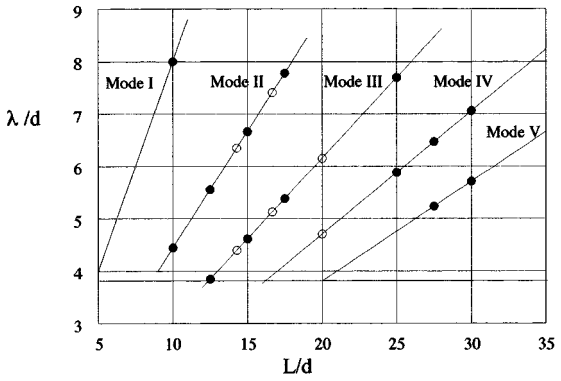

FIG. 8. Nondimensional wavelength λ/d plotted as a function of L/d. ●: varying L; ○: varying d.

values are in the range between $4d$ and $8d$ and take, in this range, values allowed by the boundary conditions. This figure explains why the oscillations do not appear always with the same mode; for example, for L/d higher than 10, the mode I is not selected, the corresponding wavelength being too high compared with the jet width d. We did not observe self-sustained oscillations for L/d higher than 35, which suggests that the system loses spatial coherence when it contains more than 5 wavelengths.

In conclusion, we argue that the nozzle width d imposes the selected wavelength band within the values allowed by the boundary conditions (imposed by the impingement length L). The wavelength value selected by the system depends mainly on the ratio L/d and on the Reynolds number. The global threshold of self-sustained oscillations depends mainly on the parameter W.

V. STUDY OF THE FREQUENCY

The period of the oscillations is obtained using the frequency extraction procedure described in Sec. II. Figure 9 represents the spatiotemporal representation of the image intensity along the line $x/d=22$ for $L/d=25$ and $\mathrm{Re}=250$. The measured periods were obtained by determining the number of pixels for 10 periods averaging on Fig. 9. We observed a variation of approximately 2 pixels for 10 periods (approximately 100 pixels) for different measurements resulting in an

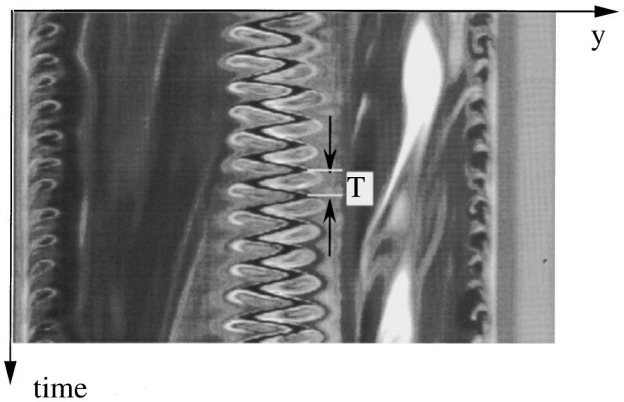

FIG. 9. Spatiotemporal acquisition of the line at $x/d=22$ for $\mathrm{Re}=250$ and $L/d=25$ (mode IV is observed).

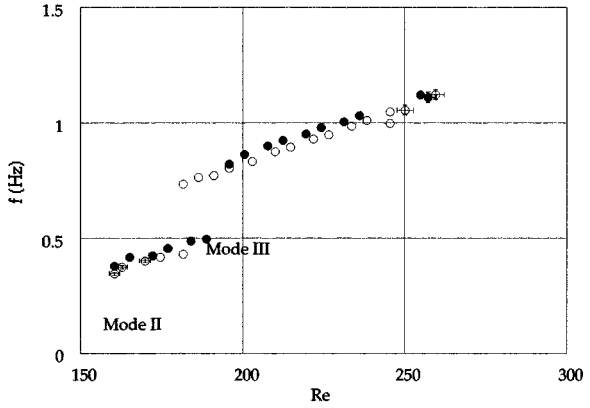

FIG. 10. Frequency vs Reynolds number for $L/d=17.5$. The symbols ○ and ● correspond to different series of measurements.

error of the order of 2%. We have measured the frequency for various downstream positions of the reference line and did not find any significant variation, thus confirming that the phenomenon is globally organized.

We have varied the Reynolds number for a given cavity configuration in the regime of self-sustained oscillations. Figure 10 shows the fundamental frequency as a function of the Reynolds number for $L/d=17.5$. It can be seen that the frequency values form separate sets grouped along straight lines corresponding to modes II and III for this value of L/d.

Similar measurements for $L/d=10$, 12.5, 15, 25, 27.5, and 30 were also performed. The frequency data were scaled with the cavity length L and the jet velocity $U_{\max}$ to form the Strouhal number $\mathrm{St}=fL/U_{\max}$ as shown in Fig. 11. The threshold for the first unstable mode observed is fairly constant and approximately equal to $\mathrm{Re}_c=160$. When the cavity length increases, the first observed mode is of higher order. For a given Reynolds number and constant mode, higher cavity length corresponds to lower frequency. The values of the Strouhal number remain nearly constant for each mode but we observe lower values for small Reynolds numbers. This last observation may be explained as follows. All the frequency data are linearly dependent on the Reynolds number over the entire range of the measurements for each mode

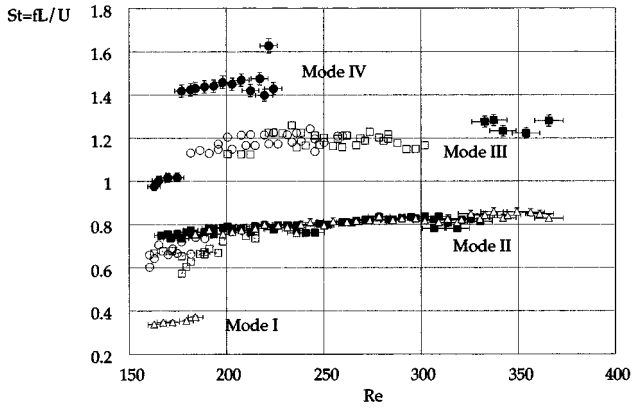

FIG. 11. Strouhal number $St=fL/U_{\max}$ vs Reynolds number. △: $L/d=10$; ■: $L/d=12.5$; □: $L/d=15$; ○: $L/d=17.5$; ●: $L/d=25$.

and can be fitted with $f=f_0+a\mathrm{Re}$, where f_0 is the frequency extrapolated to Re=0. The Strouhal number as a function of the Reynolds number is consequently not constant: it has to be corrected with a term that depends on the Reynolds number: $\mathrm{St}=f_0L/U_{\max}+\mathrm{St}_\infty$, where St_∞ represents the asymptotic value of St as Re increases. This evolution of the Strouhal number is typical in Hopf bifurcations. It can be obtained as a solution of the weakly nonlinear Landau-Stuart equation with complex coefficients as it was used to interpret the vortex shedding in wakes [29,30,31]. Similar behavior of the Strouhal number was also observed by Wooley and Karamcheti [5] for the edge-tone configuration, but they justify erroneously this fact as a consequence of the linear theory of the stability of free jets. The term $f_0L/U_{\max}$ is often neglected when the experiments are performed at high Reynolds numbers and it is widely accepted in the literature that an oscillation mode is characterized by a constant Strouhal number [13,15,19].

VI. STREAK LINES VELOCITY

We have determined the velocity of the structures of the cavity oscillations. These structures are visualized with a tracer, and therefore correspond to the streak lines. Their velocity is denoted by C_s. In the spatiotemporal representation in Fig. 6, the line slope represents the velocity of the structures, and we note that this velocity is constant, at least in the second half of the cavity. We have extended the constant slope line to the entire cavity to find global wavelength.

In the case of the hole tone, Chanaud and Powell [13] found that the wave velocity decreases from $U_{\max}$ to $0.6U_{\max}$ when the distance from the jet nozzle varies between d and $3d$. Note that this distance of three nozzle diameters corresponds to the potential core length defined for the free jet [32] equal to 3.5 times the nozzle width. In this region, Chanaud and Powell [13] have shown that the wavelength and the frequency vary. Therefore the extension of the constant slope line in the spatiotemporal representation is not justified close to the jet exit. Since this region of about $3d$ is small compared to the impingement length L we argue that it will introduce only small error in the estimation of the wavelength.

In Fig. 12 we have represented the velocity $C_s(N)$ of each mode N as a function the Reynolds number for all the values of L. Table II gives the values of $C_s(N)/U_{\max}$ for various L obtained from Fig. 12. The results suggest that, for each mode, $C_s(N)/U_{\max}$ increases with the impingement length L. This tendency is inverse to the one found by Brown [15,16] in the edge-tone configuration. In his case, the velocity of the structures is defined as the vortex velocity and his data show that the vortex velocity increases as the distance between the nozzle and the wedge decreases. Table II suggests that for a given impingement length $C_s(N)/U_{\max}$ decreases as the mode increases; in other words, smaller structures have a smaller velocity. Again, this tendency is inverse to the one observed by Brown [15,16].

For an axisymmetric free jet, Lau, Fischer, and Fuchs [33] found that the propagation velocity is equal to 60% of the jet velocity at the nozzle. In the mixing layer configuration, the wave velocity is equal to $(U_1+U_2)/2$ (U_1 and U_2 are the velocities in each region). In the confined jet, the existence

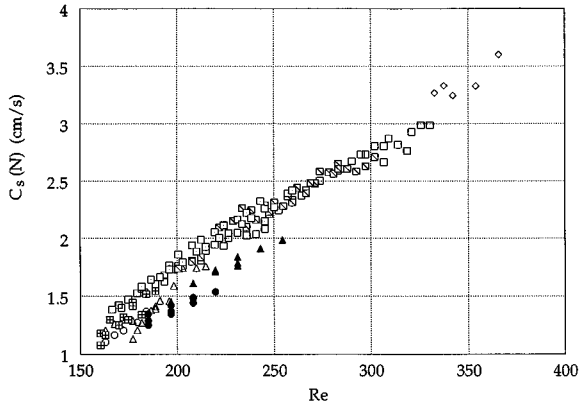

FIG. 12. Wave velocity $C_s(N)$ plotted as a function of $U_{\max}$ for N=I, II, III, IV, and V. Mode I: circles for $L/d=10$. Mode II: squares for $L/d=12.5$, triangles for $L/d=15$, squares with plusses for $L/d=17.5$. Mode III: diamonds for $L/d=12.5$, squares with diagonal lines for $L/d=15$, squares with dots for $L/d=17.5$, solid circles for $L/d=25$. Mode IV: triangles for $L/d=25$.

of a recirculating region implies a recirculating velocity $U_{\mathrm{back}}<0$, so that by analogy with mixing layers we write $C_s(N)=(U_{\max}+U_{\mathrm{back}})/2<U_{\max}/2$. In the limit of very large L, U_{back} will vanish and $C_s(N)$ will be maximal and equal to the free jet value. Therefore the results of Table II may be interpreted as follows: $U_{\mathrm{back}}/U_{\max}$ decreases as L increases, leading to a higher value of $C_s(N)$. The mean value C_s is found from Fig. 12 around $0.5U_{\max}$.

VII. VALIDITY OF THE VISUALIZATION METHOD

One of the original aspects of the present work are the results obtained from the direct measurement of the wavelength. This method presents the advantage of being nonintrusive. For example, the use of a hot wire probe can change the boundary conditions and consequently modify the selected wavelength because the probe can act as an impingement object and generates by itself a self-sustained oscillating behavior, as shown by Hussain and Zaman [21].

However, the method used here relies on visualization of the streak lines and it is well known that for an unsteady flow the streak lines and the stream lines do not coincide. Hama [26] studied numerical calculations of streak lines for a half free jet perturbed with periodic fluctuation of the amplitude. Despite the lack of coincidence between streak lines and stream lines, he showed that on center line the wavy dye pattern has a wavelength (so-called apparent wavelength) similar to the stream-line wavelength (the true wavelength). Consequently, the advancement of the dye pattern on center

TABLE II. Propagation velocity C_s for each mode N and for various values of L.

L (mm)	40	50	60	70	100
$C_s(\mathrm{I})/U_{\max}$	0.47				
$C_s(\mathrm{II})/U_{\max}$	0.42	0.40	0.50	0.54	
$C_s(\mathrm{III})/U_{\max}$		0.36	0.37	0.41	0.47
$C_s(\mathrm{IV})/U_{\max}$					0.40

line gives an apparent wave velocity identical to the true wave velocity.

In what follows we present a simple model of the oscillations of the flow field and obtain an analytical expression for the streak lines. First, we claim that the principal characteristic of such flow is the confinement in the streamwise direction that imposes boundary conditions. These boundary conditions lead to a wavelength selection, so that the proposed model includes only the spatial and temporal periodicities of the perturbation near the center line. In the model, the profile near the center line is supposed uniform and equal to U_0. In the real case the velocity near the center line is clearly not constant along the jet axis. It is approximately equal to U_{mean} at the entrance and, according to the mass conservation, decreases to $0.2U_{\text{mean}}$ at the exit of the cavity. We estimate the mean velocity U_0 as the half sum of these two values so that $U_0=0.6U_{\text{mean}}$. From the results of Sec. II, we get $U_0=0.6\times 0.9U_{\max}=0.54U_{\max}$.

For small oscillations, to the first order in the amplitude of the oscillations μ, the velocity components on the center line can be written as follows:

$$u=U_0,$$
$$v=\mu\ \cos(\omega t-kx), \tag{1}$$

where u and v are the components of the velocity in the x (streamwise) direction and the y direction (perpendicular to the jet axis), respectively. Because of the symmetry of the flow field, the u component on the symmetry axis oscillates with a double frequency and has no contribution of the first order in μ [34] and v component has no constant term (v is zero without oscillations). We have confirmed these two points numerically [24,35,36].

We consider the case where the phase velocity $c=\omega/k$ is different from U_0 (excluding the usually called critical layer). Equation (1) allows the calculation of the path-line equations with $(x_0=0, y_0=0)$ at $t=t_0$:

$$x=\int_{t_0}^{t} u\ dt=U_0(t-t_0),$$

$$y=\int_{t_0}^{t} v\ dt$$
$$=\eta\ \sin\frac{(\omega-kU_0)(t-t_0)}{2}\cos\frac{(\omega-kU_0)t+(\omega+kU_0)t_0}{2}, \tag{2}$$

where $\eta=2\epsilon/(\omega-kU_0)$ is again a small parameter if $c\neq U_0$.

By eliminating t_0 between x and y in (2), we obtain the streak-line equation for the injection point at $(x_0=0, y_0=0)$:

$$y=\eta\ \sin(K_m x)\cos(\omega t-K_s x), \tag{3}$$

where

$$K_m=\tfrac{1}{2}k(1-c/U_0) \tag{4}$$

characterizes the modulation of the streaklines envelope and

$$K_s=\tfrac{1}{2}k(1+c/U_0) \tag{5}$$

is the streak-line wave number.

Equation (3) shows that streak lines and stream lines have the same temporal periodicity. Their spatial periodicity differs, however, and we have to estimate the difference between K_s and k. A relation between the streak-line velocity $C_s=\omega/K_s$ and c is given by

$$c/U_0=\frac{C_s/U_0}{2-C_s/U_0}. \tag{6}$$

From (5) and (6), we obtain a relation between the wave numbers of the streak lines and the stream lines:

$$k=K_s(2-C_s/U_0). \tag{7}$$

From the experimental determination of C_s presented in Sec. VI, we obtain $C_s/U_0=(C_s/U_{\max})(U_{\max}/U_0)=0.5/0.54=0.94$, so that from (6), we deduce that the velocity c differs from C_s by 7.5%. In the same way, we deduce from (7) that the real wavelength of the stream line is smaller than the wavelength measured by the visualization method with the same systematic error.

The model proposed here does not include all the elements that could influence the streak-line behavior. Taking into account the change of velocity value in the streamwise direction or its dependence on the other coordinate could improve the model presented here. These elements make the calculations more complex and analytical solutions are no more possible. Bouchet *et al.* [37] have performed numerical calculations in this configuration, where the streak lines are integrated numerically along the path lines to take into account the spatial dependence of the perturbation on the transverse direction and its spatial growth in the streamwise direction, characteristic for open flows. Similar results to those presented here for the frequency and the wavelength value were found and the authors have shown that the qualitative form of the streak line and of the corresponding spatiotemporal acquisition were represented correctly and compared well with the experimental results presented here.

VIII. CONCLUSIONS

We have presented an experimental study of flow regimes observed in a rectangular cavity and described its behavior as a function of the relevant parameters: the cavity length L and width W, the nozzle width d, and the Reynolds number. A complete visualization study of self-sustained oscillations has been carried out.

We confirm the existence of discrete modes characterized, asymptotically, by a constant Strouhal number, based on the cavity length. We show that these modes, also called stages in the literature, are characterized by a constant wavelength. This wavelength is selected by the boundary conditions imposed by the cavity length. We found a wavelength selection criterion of the form $L=(N+\epsilon)\lambda$, where ϵ is close to 1/4. This empirical law is in good agreement with those found in other confined geometries [15–17]. We show that only a finite band of N values is selected from all the values admitted by the boundary conditions. This selected wavelength band is determined by the nozzle width d. We conclude that the pertinent geometrical parameter for the wavelength selection is the ratio L/d.

Using a simple analytical model, we have also performed calculations of the streak lines near the center line. The results, in agreement with the conclusions of Hama [26], show that injection of dye on the center line of the system allows an approximate determination of the true wavelength and the true wave velocity. We have shown that the use of visualization as measurement method can give accurate results in geometries where intrusive methods can change dramatically the boundary conditions of the system.

The main result of the present work is the determination of the band wavelength selection. We present the existence of a band of allowed wavelengths and report the upper and lower limit for the wavelength selection criterion. The understanding of the limits of the selected wavelength band of self-sustained oscillations remains an important open problem. We have determined the pertinent parameters for the wavelength selection as the Reynolds number and the ratio of the impingement length L to the nozzle diameter d.

Finally, new experiments should be conducted to determine the nature of the feedback necessary to excite coherent oscillations in the flow. For example, introducing a grid or a porous material in the recirculation domains could destroy the vorticity perturbations convected by the backflow. If the feedback is due to a hydrodynamic backflow, blocking it will destroy the oscillations. This work is in progress. Much interest exists in the understanding of the possible coexistence or intermitency of modes when jumps between selected modes occur. New experiments are ongoing in this direction to elucidate this open problem, by pressure measurements of the full band of excited modes, showing modes coexistence [38,39].

ACKNOWLEDGMENTS

We acknowledge support for this work provided by Schlumberger Montrouge Research. We would like to thank Souad Zikikout from GEM/Schlumberger Ind. for her collaboration in the experiments at the Schlumberger site and Philippe Petitjeans at the ESPCI. Results varying the nozzle and the cavity widths have been obtained with the help of Gilles Bouchet. We acknowledge enlightening discussions with Vincent Pagneux. We are also grateful to Raymond Poisier and Jean Claude Guibert for their work preparing the test cavity.

[1] C. Sondhauss, Ann. Phys. (Leipzig) **91**, 214 (1854).
[2] D. Rockwell and E. Naudasher, Ann. Rev. Fluid Mech. **11**, 67 (1979).
[3] W. K. Blake and A. Powell, in *Recent Advances in Aeroacoustics*, edited by A. Krothapalli and C. A. Smith (Springer, Berlin, 1986), pp. 247–335.
[4] M. Verge, B. Fabre, W. Mahu, A. Hirschberg, R. van Hassel, A. Wijnands, J. de Vries, and C. Hogendoorn, J. Acoust. Soc. Am. **95**, 1119 (1991).
[5] J. P. Woolley and K. Karamcheti, AFOSR Report No. TR-73-0503 (unpublished).
[6] J. E. Rossiter, Aeronautics Research Council, London Report & Memo. No. 3438 (unpublished).
[7] K. Yu, A. Trouve, and J. Daily, J. Fluid Mech. **232**, 47 (1991).
[8] T. Shakouchi, J. Dyn. Syst. Meas. Control **111**, 535 (1989).
[9] B. Huang, Ph. Hocquet, and P. Ligneul (unpublished).
[10] H. Sato, J. Fluid Mech. **7**, 53 (1959).
[11] E. Villermaux and E. J. Hopfinger, Physica D **72**, 230 (1994).
[12] J. W. S. Rayleigh, *The Theory of Sound* (MacMillan, New York, 1884).
[13] R. D. Chanaud and A. Powell, J. Acoust. Soc. Am. **37**, 902 (1965).
[14] C. Ho and P. Huerre, Annu. Rev. Fluid Mech. **16**, 365 (1984).
[15] G. B. Brown, Proc. R. Soc. London **49**, 439 (1937).
[16] G. B. Brown, Proc. R. Soc. London **49**, 508 (1937).
[17] A. Powell, Acustica **3**, 233 (1953).
[18] D. G. Crighton, J. Fluid Mech. **234**, 361 (1992).
[19] A. Powell, J. Acoust. Soc. Am. **33**, 395 (1961).
[20] V. Sarohia, AIAA J. **15**, 984 (1977).
[21] A. K. M. F. Hussain and K. B. M. Q. Zaman, J. Fluid Mech. **87**, 349 (1978).
[22] C. Fave, S. Soreefan, and R. Henry (unpublished).
[23] C. Ho and D. Nosseir, J. Fluid Mech. **105**, 119 (1981).
[24] A. Maurel, Ph.D. thesis, Université Paris VI–France, 1994.
[25] A. Maurel, P. Ern, and S. Zikikout (unpublished).
[26] F. R. Hama, Phys. Fluids **5**, 644 (1962).
[27] W. J. A. Dahm, and P. E. Dimotakis, AIAA J. **25**, 1216 (1987).
[28] W. J. A. Dahm and P. E. Dimotakis, J. Fluid Mech. **217**, 299 (1990).
[29] C. Mathis, M. Provansal, and L. Boyer, J. Phys. (Paris) Lett., **45**, L483 (1984).
[30] K. R. Sreenivasan, P. J. Strykowski, and D. J. Olinger, in *Proceedings of the Forum on Unsteady Flow Separation*, edited by K. N. Ghia (ASME, New York, 1987), Vol. 52, pp. 1–13.
[31] S. Raghu and P. Monkewitz, Phys. Fluids A **3**, 501 (1991).
[32] C. Ho and F. B. Hsiao, in *Structure of Complex Turbulent Shear Layers*, edited by R. Dumas and L. Fulachier (Springer, Berlin, 1983), pp. 121–136.
[33] L. C. Lau, M. J. Fischer, and H. V. Fuchs, J. Sound Vib. **22**, 379 (1972).
[34] H. Stuart, J. Fluid Mech. **4**, 1 (1958).
[35] V. Pagneux and A. Maurel, C. R. Acad. Sci. Paris **319**, 617 (1994).
[36] A. Maurel, V. Pagneux, and J. E. Wesfreid, Europhys. Lett. **32**, 217 (1995).
[37] G. Bouchet, A. Maurel, V. Pagneux, and J. E. Wesfreid (unpublished).
[38] P. Ern and J. E. Wesfreid, AIAA J. **34**, 10 (1995).
[39] G. Bouchet (unpublished).